ANTIOXIDANTS & REDOX SIGNALING
Volume 15, Number 2, 2011
© Mary Ann Liebert, Inc.
DOI: 10.1089/ars.2010.3797

ORIGINAL RESEARCH COMMUNICATION

The Pentose Phosphate Pathway Is a Metabolic Redox Sensor and Regulates Transcription During the Antioxidant Response

Antje Krüger,[1] Nana-Maria Grüning,[1] Mirjam M.C. Wamelink,[2] Martin Kerick,[1] Alexander Kirpy,[1] Dimitri Parkhomchuk,[1] Katharina Bluemlein,[1] Michal-Ruth Schweiger,[1] Aleksey Soldatov,[1] Hans Lehrach,[1] Cornelis Jakobs,[2] and Markus Ralser[1,3]

Abstract

Aims: A shift in primary carbon metabolism is the fastest response to oxidative stress. Induced within seconds, it precedes transcriptional regulation, and produces reducing equivalents in form of NADPH within the pentose phosphate pathway (PPP). ***Results:*** Here, we provide evidence for a regulatory signaling function of this metabolic transition in yeast. Several PPP-deficiencies caused abnormal accumulation of intermediate metabolites during the stress response. These PPP-deficient strains had strong growth deficits on media containing oxidants, but we observed that part of their oxidant-phenotypes were not attributable to the production of NADPH equivalents. This pointed to a second, yet unknown role of the PPP in the antioxidant response. Comparing transcriptome profiles obtained by RNA sequencing, we found gene expression profiles that resembled oxidative conditions when PPP activity was increased. *Vice versa*, deletion of PPP enzymes disturbed and delayed mRNA and protein expression during the antioxidant response. ***Innovation:*** Thus, the transient activation of the PPP is a metabolic signal required for balancing and timing gene expression upon an oxidative burst. ***Conclusion:*** Consequently, dynamic rearrangements in central carbon metabolism seem to be of major importance for eukaryotic redox sensing, and represent a novel class of dynamic gene expression regulators. *Antioxid. Redox Signal.* 15, 311–324.

Introduction

The cellular redox state, the ratio between reducing and oxidizing molecules, is tightly controlled and actively kept within a physiological range. A shift of this balance toward higher concentrations of oxidizing molecules, known as oxidative stress, is biologically deleterious and a feature of cancer and neurodegenerative disorders, but it also accompanies aging (9, 38). However, also excess of reducing equivalents is harmful, and has been implicated in human disease (30). Reductive stress appears to be problematic, as the biological system relies on a natural level of oxidant equivalents for the correct functioning of metabolic reactions, signaling, and the immune system (36, 41).

All modern organisms possess a variety of mechanisms to react upon an imbalance in the redox state. These mechanisms split into stress response processes, which grant the survival of a cell during an acute stress situation, and balancing processes, which continuously maintain the redox state and compensate naturally occurring levels of oxidants and reductants (8, 21).

Upon an oxidative burst, the eukaryotic cell slows down cell division and growth, and induces several enzymatic as

Innovation

The pentose phosphate pathway (PPP) is a known donor of NAPDH during oxidative stress conditions. Here, we provide evidence for a second role of the pathway during the antistress response. The deletion of yeast PPP enzymes caused growth phenotypes on oxidant-containing media that were not attributable to aberrant NADPH formation, and had defects in the regulation of gene expression upon an oxidant-treatment. Since augmented PPP flux provoked gene expression profiles that resembled oxidative stress conditions, it can be concluded that the PPP is a metabolic redox sensor and involved in adapting the transcriptome to counteract oxidative stress.

[1]Max Planck Institute for Molecular Genetics, Berlin, Germany.
[2]Metabolic Unit, Department of Clinical Chemistry, VU University Medical Center, Amsterdam, The Netherlands.
[3]Department of Biochemistry, Cambridge Systems Biology Centre, University of Cambridge, Cambridge, United Kingdom.

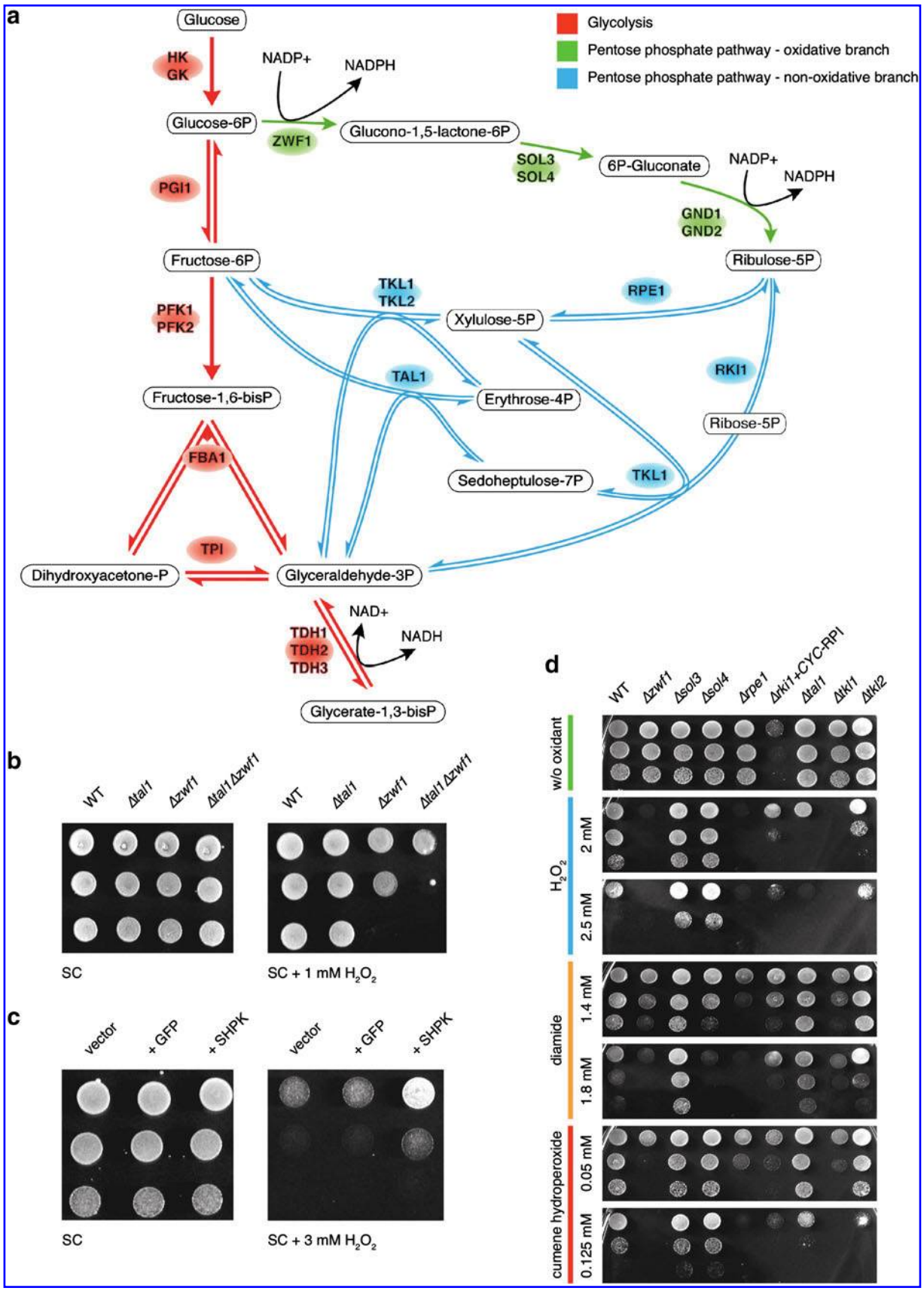
a
Glycolysis
Pentose phosphate pathway - oxidative branch
Pentose phosphate pathway - non-oxidative branch
Glucose
HK
GK
NADP+
NADPH
Glucose-6P
ZWF1
Glucono-1,5-lactone-6P
SOL3
SOL4
6P-Gluconate
NADP+
NADPH
PGI1
GND1
GND2
Fructose-6P
Ribulose-5P
TKL1
TKL2
RPE1
PFK1
PFK2
Xylulose-5P
TAL1
RKI1
Fructose-1,6-bisP
Erythrose-4P
Ribose-5P
FBA1
Sedoheptulose-7P
TKL1
TPI
Dihydroxyacetone-P
Glyceraldehyde-3P
NAD+
NADH
TDH1
TDH2
TDH3
Glycerate-1,3-bisP
b
WT
Δtal1
Δzwf1
Δtal1Δzwf1
SC
SC + 1 mM H2O2
c
vector
+ GFP
+ SHPK
SC
SC + 3 mM H2O2
d
WT
Δzwf1
Δsol3
Δsol4
Δrpe1
Δrki1+CYC-RPI
Δtal1
Δtkl1
Δtkl2
w/o oxidant
H2O2
2 mM
2.5 mM
diamide
1.4 mM
1.8 mM
cumene hydroperoxide
0.05 mM
0.125 mM

well as nonenzymatic antioxidative defense systems. These processes help to restore the natural redox balance (21, 24), and repair damage that has already occurred (24, 40). Although many biochemical details of the defense systems have been elucidated, the sensor systems that monitor the redox state and are responsible for induction and control of the redox-state balancers are only marginally understood. The best studied mechanism is the transcriptional induction of stress response genes *via* transcription factors that are regulated by redox-sensing cysteines. The oxidation of the thiol function in cysteine, whether directly or indirectly by the transfer of redox equivalents from a regulatory interaction partner (such as the glutathione peroxidase 3 [Gpx3]), induces the expression of antioxidant enzymes (3, 15, 41). However, such a system is not capable of responding to stress caused by reducing agents and this indicates that additional sensors exist.

Beside transcriptome and proteome, also the metabolome has been identified as an integral component of the cellular stress defense machinery (12). A major target under oxidative conditions is the pentose phosphate pathway (PPP), a pathway in primary carbon metabolism that is closely interconnected with glycolysis. The PPP divides into an oxidative and a nonoxidative branch, two independently operating metabolic modules (45) (Fig. 1a, and Table 1 for overview of reactions/enzymes). The oxidative branch is composed of irreversible reactions and reduces $NADP^+$ to NADPH. In contrast, reactions of the nonoxidative branch are reversible, and neither NAD(H) nor NADP(H) dependent.

Treatment with an oxidant blocks glycolysis, but glucose uptake continues, leading to an increased metabolic load of the redox-resistant PPP during the initial phase of the stress response (16, 33, 37). Yeast cells exposed to hydrogen peroxide (H_2O_2) show a strong increase in the concentration of PPP intermediates. In addition, oxidative treatments induce PPP enzymes on transcript and protein levels (7, 10, 37). The benefits of this metabolic transition are presently explained by the production of NADPH in the oxidative PPP branch, the primary redox-cofactor for glutathione synthesis and for enzymes of the antioxidative machinery (11, 17, 29). Cells with an increased influx to the PPP have a higher NADPH/$NADP^+$ ratio and are more resistant to oxidants (33). *Vice versa*, deletion of the first and rate limiting enzyme of the oxidative PPP, the glucose 6-phosphate dehydrogenase (G6PDH, Zwf1 [ZWischenFerment]), causes hypersensitivity to multiple oxidants in various organisms (14, 17). The redox-protective effects of the PPP are also diminished when the NADPH oxidizing enzyme *GDP1* (an NADP(H)-dependent form of glyceraldehyde-phosphate dehydrogenase found in the fungus *Kluyveromyces lactis*) is expressed (33, 42). Castegna and colleagues determined NADPH/$NADP^+$ ratios in wild-type and Δ*zwf1* cells, without and upon the addition of H_2O_2, by liquid chromatography tandem mass spectrometry (LC-MS/MS). In the wild-type strain, NADPH/$NADP^+$ ratio fall from 1.5 to ~1.0 after adding H_2O_2 for 60 min. The Δ*zwf1* mutant had a ratio of 1.0, which collapsed to < 0.2 when exposed to H_2O_2 (4). Hence, NADPH is not sufficiently recovered in cells deficient for the oxidative PPP when exposed to H_2O_2.

Here, we demonstrate that the PPP has a second function in the oxidative stress response. We describe redox phenotypes of PPP enzyme mutants that are not a result of altered NADPH metabolism, and found evidence that the PPP is an integral component of the gene expression regulome during stress conditions. Our data, showing disturbed regulation of gene expression during the stress response in PPP deficient yeast, support the hypothesis of PPP being a metabolic redox sensor. Further, we provide evidence that the glycolysis/PPP transition is essential for functioning timing of antioxidative mRNA and protein expression.

Results

An NADP(H)-independent role of the PPP during the antioxidant response

The requirement of the PPP during the oxidative stress response has been explained with its function as source of redox equivalents in form of NADPH. However, even though NADPH is solely produced in the oxidative branch of the PPP, sensitivity toward oxidants has also been reported for mutants deficient in nonoxidative PPP enzymes (17). Further, in our previous LC-MS/MS studies we observed accumulation of nonoxidative PPP intermediates upon exposing cells to oxidants (33, 34). Together, these observations indicated that the involvement of the PPP in the stress response might go beyond its function as NADPH donor.

To investigate this hypothesis, we first generated double-deletion strains lacking one of the nonoxidative PPP enzymes, *TKL1*, *RPE1*, or *TAL1*, and the limiting entry enzyme of the oxidative PPP (Zwf1). Since the oxidative part of the PPP is not reversible, Δ*zwf1* strains cannot use the PPP to reduce $NADP^+$. Δ*tkl1*Δ*zwf1* and Δ*rpe1*Δ*zwf1* double mutants were not viable (Supplementary Fig. S1; Supplementary data are available online at www.liebertonline.com/ars); thus, only

FIG. 1. A redox-independent role of the pentose phosphate pathway (PPP) during the oxidative stress response. (a) Overview of upper glycolysis, the oxidative, and the nonoxidative branch of the PPP. Glycolysis (when the PFK reaction is reversed by fructose 1,6-bisphosphatase during gluconeogenesis) and the nonoxidative PPP are reversible, whereas the oxidative PPP is irreversible. $NADP^+$ is reduced to NADPH in the oxidative PPP branch. **(b)** The nonoxidative PPP influences yeast's hydrogen peroxide (H_2O_2) resistance. Equal amounts of isogenic wild-type, *Δtal1*, *Δzwf1*, and *Δzwf1Δtal1* yeast were spotted as serial dilutions (1:1, 1:5, and 1:25 from top to bottom) onto H_2O_2-containing agar plates and imaged after 3 days incubation. The *Δzwf1Δtal1* double-knockout is more sensitive to H_2O_2 as *Δzwf1* and *Δtal1* yeast. **(c)** Yeast expressing a sedoheptulose-7P forming enzyme is resistant to H_2O_2. Yeast expressing mouse sedoheptulokinase (SHPK) that generates sedoheptulose-7P from the non-PPP sugar sedoheptulose, or controls carrying the empty vector, or a control vector expressing GFP, is spotted as serial dilution onto H_2O_2-containing agar plates and imaged after a 3-day incubation. **(d)** PPP enzyme deletion strains of both pathway branches have specific redox phenotypes. Equal amounts of wild-type cells, and isogenic mutants deleted for both oxidative and nonoxidative PPP enzymes were spotted as serial dilutions on oxidant-containing agar plates and grown for 3 days. **(b–d)** To illustrate both sensitivity and resistance phenotypes, two concentrations are shown for each oxidant. (To see this illustration in color the reader is referred to the web version of this article at www.liebertonline.com/ars).

Table 1. Overview Pentose Phosphate Pathway

Enzyme name	*Reaction catalyzed*	*Yeast enzyme nomenclature*	*Branch*
Glucose 6-phosphate dehydrogenase	Glucose 6-phosphate + NADP + → 6-phosphoglucono-δ-lactone + NADPH	Zwf1	Oxidative
6-Phosphoglucono lactonase	6-Phosphoglucono-δ-lactone + H_2O → 6-phosphogluconate + H^+	Sol3 Sol4	Oxidative
6-Phosphogluconate dehydrogenase	6-Phosphogluconate + $NADP^+$ → ribulose 5-phosphate + NADPH + CO_2	Gnd1 Gnd2	Oxidative
Ribose 5-phosphate isomerase	Ribulose 5-phosphate ↔ ribose 5-phosphate	Rki1	Nonoxidative
Ribose 5-phosphate 3-epimerase	Ribulose 5-phosphate ↔ xylulose 5-phosphate	Rpe1	Nonoxidative
Transaldolase	Sedoheptulose 7-phosphate + glyceraldehyde 3-phosphate ↔ erythrose 4-phosphate + fructose 6-phosphate	Tal1 Nqm1	Nonoxidative
Transketolase	Xylulose 5-phosphate + erythrose 4-phosphate ↔ glyceraldehyde 3-phosphate + fructose 6-phosphate	Tkl1 Tkl2	Nonoxidative
Transketolase	Xylulose 5-phosphate + ribose 5-phosphate ↔ glyceraldehyde 3-phosphate + sedoheptulose 7-phosphate	Tkl1	Nonoxidative

the Δ*tal1*Δ*zwf1* double-knockout could be assayed for its oxidant tolerance. As shown in Figure 1b, the Δ*tal1*Δ*zwf1* strain was more sensitive to H_2O_2 as both single mutants, demonstrating additive effects of the phenotypes. Thus, deletion of *TAL1* decreases the oxidant tolerances of yeast, which cannot use the oxidative PPP for NADPH regeneration.

Complementary to this experiment, we then increased the flow into the non-oxidative PPP by transgenic expression of sedoheptulokinase (SHPK). SHPK is a mammalian enzyme, not present in yeast, and converts the non-PPP sugar sedoheptulose to the central nonoxidative PPP intermediate sedoheptulose 7-phosphate (18). As illustrated in Figure 1c, yeast cells having this second route to produce nonoxidative PPP intermediates were more resistant to H_2O_2 treatment than wild-type cells and isogenic controls expressing GFP. Thus, distortion of the nonoxidative PPP decreased the cellular tolerance to H_2O_2, whereas additional flow into this pathway resulted in an increased redox tolerance.

The investigations were continued by comparing the resistance of various PPP deletion mutants to multiple oxidants. Oxidants vary in respect of their primary targets and redox (Nernst) potential, and therefore, each compound triggers a specific cellular response (39). This raised the question whether the deletion of oxidative and nonoxidative PPP enzymes provokes divergent/specific or similar redox phenotypes. Isogenic mutants of both the oxidative (*zwf1*, *sol3*, and *sol4*) and the nonoxidative (*rpe1*, *rki1*, *tal1*, *tkl1*, and *tkl2*) PPP branches were spotted as serial dilution series on agar plates with increasing concentration of the oxidants H_2O_2, diamide, and cumene-hydroperoxide (CHP). As shown in Figure 1d, yeast strains deleted for *zwf1*, *rpe1*, and *tkl1* were sensitive to the three tested oxidants; *Δtkl2* and *Δsol4* selectively to at least one. In contrast, lack of *sol3* increased the overall oxidant tolerance. The remaining strains had divergent phenotypes: *Δtal1* cells were sensitive H_2O_2 but resistant to diamide, *Δsol4* cells were resistant to H_2O_2 and CHP, but sensitive to diamide. A strain with lowered ribose 5-phosphate isomerase (RPI) activity [a Δ*rki1* knockout is unviable, the strain with reduced Rpi activity was engineered by low-level expression of the human Rki1p ortholog *RPI1A* in a *RKI1* null strain (44)] showed slow growth on control plates, but its growth was largely unaffected by the oxidant treatments.

To test if these phenotypes were specific to oxidants, we tested the resistance of Δ*zwf1*, Δ*sol3*, Δ*sol4*, Δ*rpe1*, Δ*tal1*, Δ*tkl1*, and Δ*tkl2* yeast against other stressors. The strains were spotted on media with different concentrations of dithiothreitol (DTT) to simulate a reductive stress, NaCl for salt stress, sorbitol for osmotic stress, and $MnCl_2$ for a heavy metal stress. Except slight growth advantages on NaCl, no other stress phenotypes of PPP deletion strains were observed (Supplementary Fig. S2). Further, we measured the ratio of [NADPH] to [$NADP^+$ + NADPH] (=$NADPH_{total}$) in cell extracts of nonoxidative PPP knockout strains. These ratios were unchanged compared to wild-type under the chosen growth conditions, indicating that the altered oxidant resistance of nonoxidative PPP knockouts is not the result of lack or excess of NADPH (Supplementary Fig. S3).

In summary, depletion of both oxidative and nonoxidative PPP enzymes strongly affected oxidant resistance of yeast, but did not cause broad growth phenotypes with unrelated stressors. Remarkably, depleting enzymes of both PPP branches produced specific phenotypes. For instance, *Δtal1* yeast was sensitive to H_2O_2, resistant to diamide, and tolerated CHP like the wild-type. A comparable phenotype was not seen among deletion strains of oxidative PPP enzymes.

Taken these findings together, it could be demonstrated that the PPP plays a specific role in the oxidative stress response, and that not only its NADPH-producing oxidative branch but also its nonoxidative part is required for maintaining the natural oxidant tolerance of yeast. It was therefore concluded that the function of the PPP in stress response is not restricted to provide NADPH.

Redox-sensitive mutants accumulate nonoxidative PPP intermediates upon an oxidative burst

To investigate whether redox sensitivity of non-$NADP^+$ reducing PPP deletion mutants correlates with metabolic changes, which occur during the stress response, six PPP intermediates were quantified using LC-MS/MS. The three most redox-sensitive nonoxidative PPP deletion strains (*Δrpe1*, *Δtal1*, and *Δtkl1*) as well as the most resistant (*Δsol3*) strain and their wild-type parent BY4741 were profiled. Additionally, these metabolites were quantified after exposure to H_2O_2. As reported earlier (33), H_2O_2 treatment triggered an increase in the concentrations of PPP intermediates in the wild-type strain. Similar metabolic changes were observed in *Δsol3* yeast (Fig. 2). However, this response was substantially different in Δ*tal1*, Δ*rpe1*, and Δ*tkl1* cells. Here, PPP intermediates 6-phosphogluconate, ribose 5-phosphate, and sedoheptulose 7-phosphate accumulated up to 100-fold compared to the wild-type. Thus, it can be deduced that a block in the nonoxidative PPP, which causes oxidant sensitivity, has a strong impact on the concentration of its intermediates during an acute stress response.

The glycolysis/PPP transition induces transcriptional rearrangements that are part of the antioxidant response

The glycolysis/PPP transition is induced very quickly; a raise in the concentration of PPP intermediates is detected within seconds after the oxidative burst. This fast induction is attributable to oxidative inactivation of glycolytic enzymes (34, 37). Since changes in transcript levels are detected much later (minutes) (7) and metabolic pathways are in intensive crosstalk with the gene expression machinery (12), we speculated that the early metabolic shift could be connected to the regulation of gene expression during the stress response.

To pursue this hypothesis, we profiled the transcriptome of a mutant yeast strain (MR105) that has increased activity of the PPP due to reduced activity of a central glycolytic enzyme, triosephosphate isomerase (*Tpi1*).

MR105 is deleted for endogeneous *TPI1*, and expresses a mutant allele ($TPI_{Ile170Val}$) from a centromeric plasmid (31). The $TPI_{Ile170Val}$ allele, identified as heterozygous polymorphism in TPI deficiency (1), has 30% of the wild-type TPI activity. Previously, we have shown that PPP intermediates are increased in MR105, and found that this strain is resistant

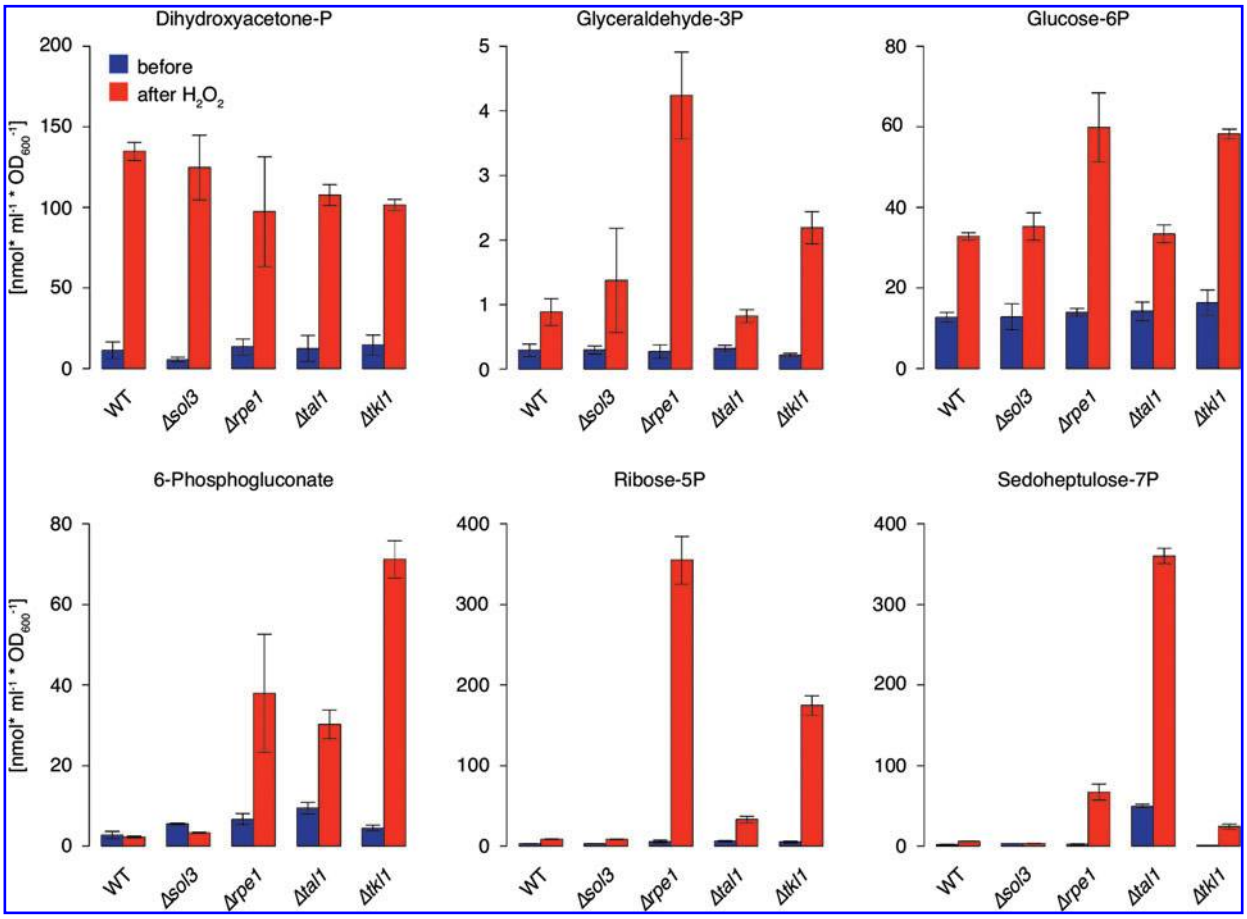

FIG. 2. Oxidant-sensitive PPP deletion strains accumulate PPP intermediates upon an oxidative burst. Glycolytic/PPP intermediates were quantified by liquid chromatography tandem mass spectrometry (LC-MS/MS) in oxidant-treated (*red*) and untreated (*blue*) yeast strains. Values are given in nmol/ml normalized to relative yeast biomass. Error bars indicate the standard deviation from four measurements from two yeast batch cultures. (To see this illustration in color the reader is referred to the web version of this article at www.liebertonline.com/ars).

to oxidants and has an increased NADPH/$NADP^+$ ratio (31, 33).

The transcriptome analysis was performed to compare changes in gene expression that follow the activation of the PPP, induced by the TPI mutation or by H_2O_2 exposure. Global mRNA expression profiles were obtained by quantitative shotgun sequencing on a Genome Analyzer II (Illumina). The wild-type strain with and without H_2O_2, the MR105 strain, and yeast strains deleted for the PPP enzymes *Tal1*, *Tkl1*, and *Zwf1* were profiled. cDNA was synthesized from total RNA using an oligo-dT primer and processed to obtain strand-specific sequencing profiles, which were obtained using a 51-bp paired-end sequencing-by-synthesis approach as described earlier (26). Each experiment yielded 10–14 million single

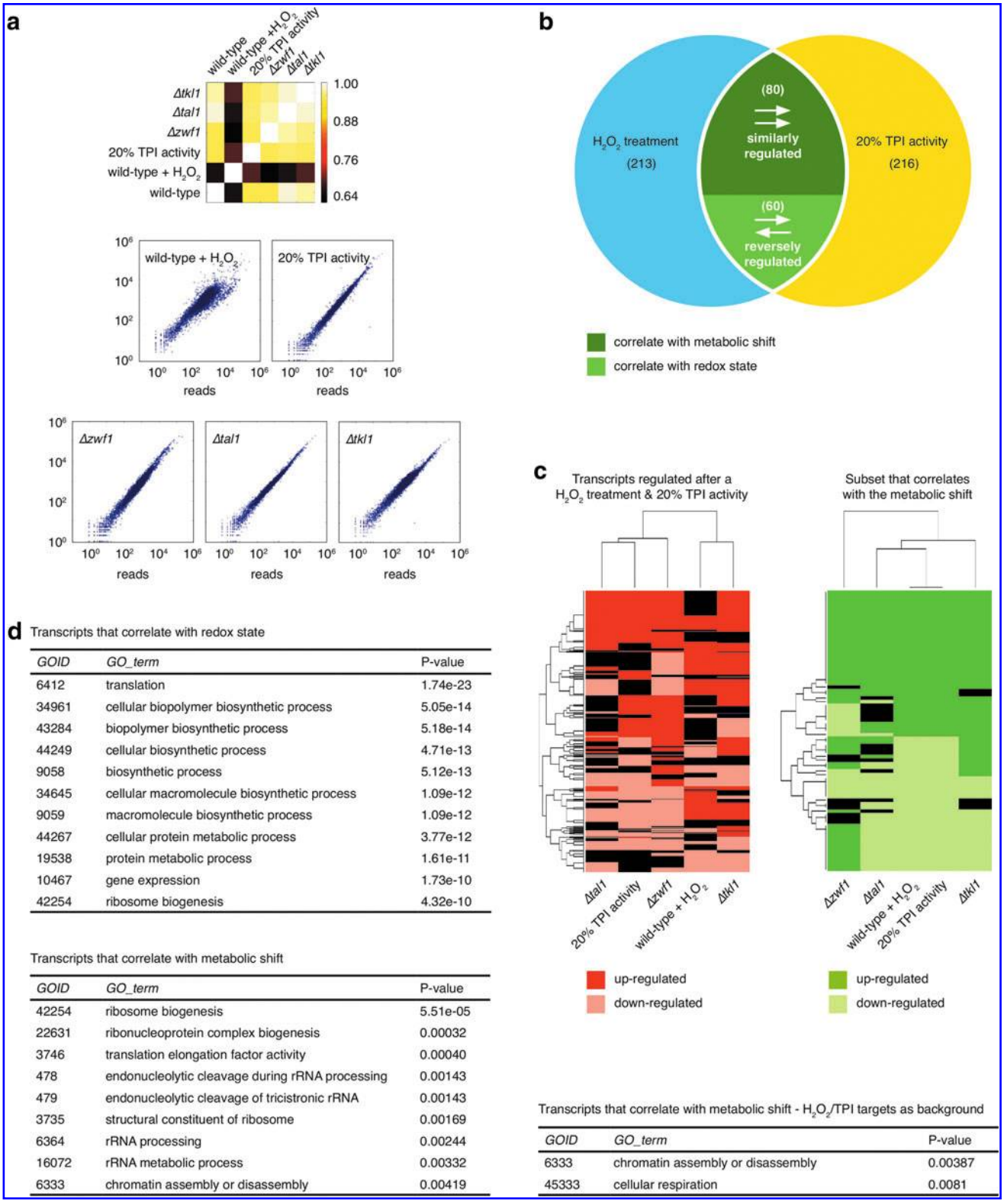

d Transcripts that correlate with redox state

GOID	GO_term	P-value
6412	translation	1.74e-23
34961	cellular biopolymer biosynthetic process	5.05e-14
43284	biopolymer biosynthetic process	5.18e-14
44249	cellular biosynthetic process	4.71e-13
9058	biosynthetic process	5.12e-13
34645	cellular macromolecule biosynthetic process	1.09e-12
9059	macromolecule biosynthetic process	1.09e-12
44267	cellular protein metabolic process	3.77e-12
19538	protein metabolic process	1.61e-11
10467	gene expression	1.73e-10
42254	ribosome biogenesis	4.32e-10

Transcripts that correlate with metabolic shift

GOID	GO_term	P-value
42254	ribosome biogenesis	5.51e-05
22631	ribonucleoprotein complex biogenesis	0.00032
3746	translation elongation factor activity	0.00040
478	endonucleolytic cleavage during rRNA processing	0.00143
479	endonucleolytic cleavage of tricistronic rRNA	0.00143
3735	structural constituent of ribosome	0.00169
6364	rRNA processing	0.00244
16072	rRNA metabolic process	0.00332
6333	chromatin assembly or disassembly	0.00419

Transcripts that correlate with metabolic shift - H_2O_2/TPI targets as background

GOID	GO_term	P-value
6333	chromatin assembly or disassembly	0.00387
45333	cellular respiration	0.0081

reads, which could be aligned to 97% of the annotated yeast open reading frames. Compared to the mutant strains, grown without interruption, the oxidant treatment caused broader rearrangements in the transcriptome as illustrated by Pearson's pairwise correlation of all profiles (Fig. 3a, upper panel) and individual scatter plots (lower panel). By normalizing the transcriptome of the TPI mutant MR105 and the H_2O_2-treated strain, significant overlaps of the transcriptome profiles were detected. About 40% of the targeted genes were shared between the TPI mutant and the H_2O_2-treated strain (Fig. 3b). These two unrelated conditions, both increasing the concentration of PPP intermediates, triggered expression changes in an overlapping number of genes.

Whereas H_2O_2 treatment creates an oxidative environment, a drop in TPI activity shifts the $NADPH/NADP^+$ ratio toward a reducing environment (33). Therefore, it was possible that this overlap was an indirect consequence of redox-balancing processes. However, it was found that only 60 of the 140 transcripts correlated directly with the redox state (were upregulated in the H_2O_2-treated sample and downregulated in the TPI mutant or *vice versa* [Fig. 3b]). The larger number of transcripts (80), however, responded equally to the H_2O_2 treatment and the reduced TPI activation. Thus, a large fraction of the transcriptional changes seen upon H_2O_2 treatment did not directly correlate with the redox state, but with the shift in primary carbon metabolism.

The expression tendency of these genes in the PPP deletion strains was studied to assess whether their regulation was a consequence of altered PPP activity. The RNASeq expression profiles of *Δtal1*, *Δtkl1*, and *Δzwf1* yeast were hierarchically clustered with the profiles of the genes regulated upon a H_2O_2 treatment or in the TPI mutant. Interestingly, a substantial fraction of transcripts targeted by H_2O_2 treatment were also found targeted in the PPP mutants (Fig. 3c). We noticed that the profile of this set of genes in *Δtkl1* cells clustered closer to the H_2O_2 profile than the TPI strain profile (Fig. 3c, left panel). To exclude the potential effects of a changing redox state, we narrowed the analysis to transcripts regulated similarly in the TPI and H_2O_2 profiles (Fig. 3c, right panel) and detected strong overlap between the TPI/H_2O_2 set and the PPP deletion strains: 71% of the transcripts correlating with the activation of the PPP were found altered in all three, and 92% in at least two, of the profiled PPP deletion strains. This demonstrates that transcriptional changes induced by H_2O_2, which correlate with a shift in primary carbon metabolism, respond to a depletion of PPP enzymes. By performing a gene ontology (GO) comparison of these transcripts, using the targets of reduced TPI activity and H_2O_2 as background set, GO IDs 6333 (chromatin assembly and disassembly) and 45333 (cellular respiration) were found to be enriched ($p < 0.01$, Fig. 3c, lower panel). The other gene sets implicate the metabolic transition in the regulation of protein biosynthesis. Comparing the list of all redox-state correlating transcripts using the entire transcriptome as background, GO terms relating to translation and protein biosynthesis were enriched (Fig. 3d, upper panel). Reversely, transcripts directly responding to the metabolic transition were enriched for its preceding processes, namely, the assembly and biosynthesis of ribosomes (Fig. 3d, lower panel).

The metabolic transition regulates the expression of respiratory chain and chromatin components during the stress response

With given evidence for a role of the PPP in transcriptional regulation upon an oxidative burst, it was then examined how the targeted transcripts may behave upon its perturbation. The expression of identified targets belonging to the two enriched GO categories (Fig. 3c), cellular respiration (transcripts *COX1*, *COX2*, *COX3*, and *CIT1*) and chromatin assembly and disassembly (transcripts *HHT1+2*, *HTA1+2*, *HHF1+2*, and *HHO1*), was analyzed by quantitative real-time-polymerase chain reaction (qRT-PCR) and targeted proteomics. Control transcripts for internal normalization (*ACN9*, *ATG27*, and *TAF10*) were selected from the RNASeq data, fulfilling the criteria that they were minimal affected in their expression levels, neither by the H_2O_2 treatment nor by the TPI- or PPP mutations. Triplicate time courses for the expression of all transcripts in exponentially growing wild-type, Δ*zwf1*, Δ*tkl1*, and Δ*tal1* strains were generated by determining their relative expression levels before and 3, 5, 10, 15, and 30 min upon the addition of H_2O_2. The relative expression levels were normalized to the geometric mean of the $E^{\Delta Ct}$ values of three reference transcripts (28).

The H_2O_2 treatment provoked downregulation of mitochondrial-encoded cytochrome c oxidase (*COX*) genes to ~50% of their initial level in wild-type cells, whereas citrate synthase (*CIT1*) was virtually unaffected for 15 min (Fig. 4a, upper panel).

Remarkably, the expression courses of these transcripts were strongly disturbed in the PPP deletion strains (Fig 4a, lower panels). In Δ*zwf1* yeast, *COX2* and *COX3* mRNAs lost ~80% of their initial levels within 10 min. At the same time,

FIG. 3. Activation of the PPP mediates transcriptional regulation during the stress response. (a) Expression profiling by transcriptome sequencing. *Upper panel*: Pearson's pairwise correlation of the strand-specific RNAseq expression profiles of H_2O_2-treated yeast, a TPI mutant (MR105), and PPP-deletion strains. *Lower panel*: Scatter plots of RNASeq expression levels of oxidant treated/mutant yeast (*Y*-axis) in comparison to untreated wild-type yeast (*X*-axis). Values indicate normalized numbers of sequence reads per transcript. **(b)** H_2O_2 treatment and an increase in PPP activity target an overlapping set of genes. Transcripts regulated upon a H_2O_2 treatment (*blue*) and reduced TPI activity (*yellow*). Shared targets divide in reversely regulated genes that correlate with the redox state (*lime green*) or that do not correlate with the redox state but with the metabolic shift (*dark green*). **(c)** Transcripts that correlate with the metabolic shift respond to PPP deficiencies. *Left panel*: Clustering of PPP enzyme deletion strains expression profiles to transcripts regulated upon a H_2O_2 treatment and reduced TPI activity. Upregulated transcripts are shown in *red*, and downregulated in *pink*. *Right panel*: Similar analysis taking into account only the transcripts that correlated with the metabolic shift. Upregulated transcripts in *dark green*, and downregulated in *lime green*. *Lower panel*: Gene ontology (GO) analysis comparing transcripts that respond to the metabolic shift using the set of genes targeted by H_2O_2 and reduced TPI activity as background. **(d)** Activation of the PPP targets components associated with translation and ribosome biogenesis. GO term enrichment analysis of target transcripts that correlated with the redox state (*upper panel*) and the metabolic shift (*lower panel*). (To see this illustration in color the reader is referred to the web version of this article at www.liebertonline.com/ars).

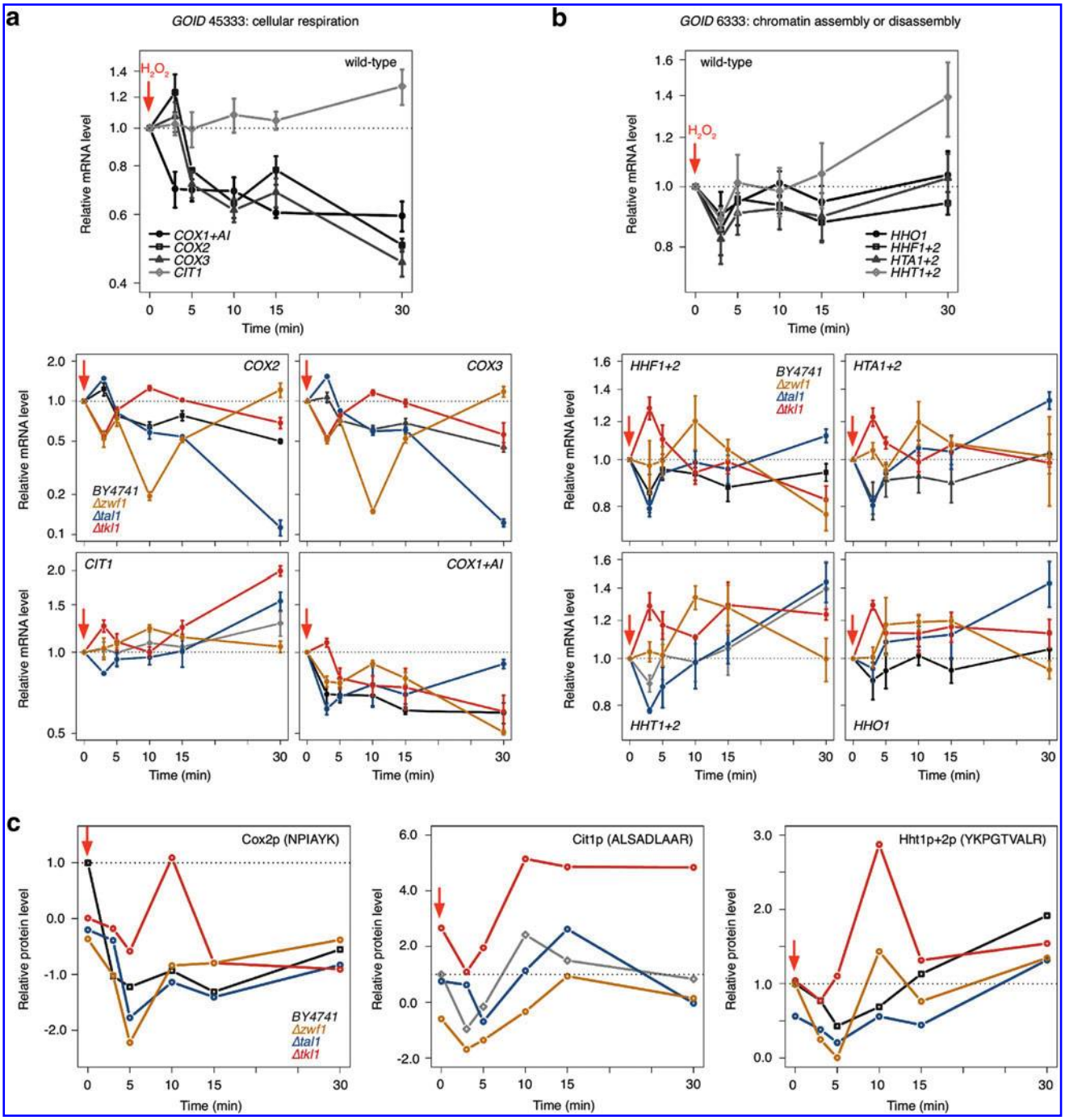

FIG. 4. Regulation of respiratory metabolism and chromatin components during the stress response depends on the PPP. (a) mRNA expression of respiratory components during the stress response in wild-type and PPP enzyme deletion mutants. (*Upper panel*) Time courses of *CIT1*, *COX1*, *COX2*, and *COX3* expression were generated by quantitative real-time-polymerase chain reaction (qRT-PCR) in wild-type yeast treated with H_2O_2 for 0, 3, 5, 10, 15, and 30 min. (*Lower panel*) Expression level time-courses as above, but obtained from Δ*zwf1* (*yellow*), Δ*tal1* (*blue*), and Δ*tkl1* (*red*) yeast. Wild-type trends are given in *gray tones*. **(b)** Histone mRNA expression during the stress response in wild-type and PPP enzyme deletion mutants (*upper panel*). Paralog transcripts follow similar trends in oxidant-treated wild-type yeast, as shown by qRT-PCR. (*Lower panel*) mRNA expression in yeast cells deleted for PPP enzymes Δ*zwf1* (*yellow*), Δ*tal1* (*blue*), and Δ*tkl1* (*red*) in comparison to the wild-type courses (*gray tones*). **(c)** Quantification of a Cox2p, a Cit1p, and a Hhtp-specific peptide in time-course experiments performed with wild-type and PPP deletion mutants. Relative abundances of peptides specific for (i) cytochrome c oxidase subunit Cox2p (left), (ii) citrate synthase Cit1p (middle), and (iii) histone Hht1p + Hht2p (right) were determined in yeast treated for 0, 3, 5, 10, 15, and 30 min by nanoLC-MS/MS using multiple reaction monitoring (MRM). These time courses were performed with wild-type (*gray*), Δ*zwf1* (*yellow*), Δ*tal1* (*blue*), and Δ*tkl1* (*red*) cells. Obtained peptide concentrations were normalized to an RPL36B-specific peptide used as internal reference. Given is the mean relative peak area of two normalized coeluting Q1/Q3 (MRM) transitions. (To see this illustration in color the reader is referred to the web version of this article at www.liebertonline.com/ars).

these transcripts were upregulated in the Δ*tkl1* strain. In contrast, in *Δtal1* yeast, *COX3*, *COX2*, and *COX1* transcripts [the latter also encodes for a reverse transcriptase AI (19)], maintained the wild-type trend for 15 min, but then their expression levels dropped drastically. The time courses for *CIT1* were primarily affected by the removal of *TAL1* and *TKL1*. In these strains, *CIT1* accumulated stronger and faster than in the wild-type situation.

In the next step, a mass Western approach was used to verify whether these transcriptional changes were also represented on protein level. Multiple reaction monitoring (MRM) experiments with internal normalization were performed on a nanoLC system coupled to a triple quadrupole/hybrid ion trap mass spectrometer (QTRAP5500) as described earlier (2). A Cox2p and a Cit1p-specific peptide was quantified in wild-type, Δ*zwf1*, Δ*tkl1*, and Δ*tal1* strains upon H_2O_2 treatment for 0, 3, 5, 10, 15, and 30 min.

As shown in Figure 4c, like the corresponding transcripts, the abundance of Cox2p and Cit1p specific peptides were affected by the deletion of PPP enzymes. The protein expression trend was much more stable in the wild-type strain. The concentration varied strongly in the PPP mutants, or was delayed as in the case of *CIT1* transcript levels in Δ*tal1* cells.

To further corroborate the influence of PPP deletions in oxidant-induced gene expression, a similar analysis was performed with members of the second enriched GO term, chromatin assembly and disassembly, containing yeast histone genes. In difference to metazoans, yeast histone transcripts are polyadenylated and are therefore present in oligo-dT-primed cDNA. Figure 4b illustrates the wild-type time-course of histone mRNA expression upon the addition of H_2O_2 to an exponentially growing yeast culture. In the wild-type strain, changes in histone gene expression were very moderate. Transcripts encoding *HTA1+2* (analyzed with a primer pair that amplifies both paralogs), *HHF1+2* and *HHO1*, exhibited a slight decline in their expression directly upon the addition of the oxidant. Their levels then stabilized rapidly and returned to basal levels. The trend in *HHT1+2* expression levels was identical during the first minutes, but then increased slightly and continuously until the end of the experiment.

Depletion of PPP enzymes also disturbed their time-course. At time points < 10 min (= all histone mRNAs were decreased in the wild-type), they were increased in *Δtkl1* cell; after 10 min, all PPP deletion strains showed abnormalities in their expression trends. After 30 min (i) *HTA1+2* transcripts were at wild-type levels, (ii) *HHF1+2* transcripts were downregulated, or (iii) upregulated (*HHT1+2* and *HHO1+2* transcripts). Their course in *Δzwf1* cells was comparable, but regulation of histone mRNA expression in this strain had a delayed onset. The *Δtal1* course, which followed the wild-type trend initially, was above wild-type levels in the end of the experiment.

Thus, alike transcripts of respiratory metabolism, stress-induced regulation of histone mRNA expression was disturbed upon the depletion of PPP enzymes. Although the relative differences in expression level were moderate when compared to those of the respiratory metabolism components, they were pictured on the protein level. In the wild-type strain, the level of an Hht1p+2p-specific peptide decreased during the first 10 min after addition of the oxidant, then stabilized, and reached wild-type levels and more (Fig. 4c, right panel). In contrast, in Δ*tkl1* and Δ*zwf1* yeast, the Htt-peptide accumulated and reached a maximal signal 10 min after the oxidative burst, and returned to a wild-type-like concentration at min 15–30.

In summary, the different time-course experiments reveal defects in timing and induction of gene expression during the stress response when different steps of the nonoxidative PPP are disturbed. Thus, the activation of the PPP, which occurs upon an oxidative burst, is required for accurate regulation of gene expression during the stress response.

Discussion

The metabolic network is of modular architecture and closely interconnected with transcriptional machinery (12, 13). This is necessary to balance metabolic perturbations or to react to a changing nutrient status, and thus changes in the metabolic network can stimulate the transcriptome and proteome (5, 12, 13). Recent discoveries unveil the metabolic network as an integral component of the cellular signaling system, and it is becoming clear that metabolic control goes far beyond self-regulation of metabolic pathways. For instance, it has recently been shown that inhibition of the eicosanoid pathway promotes pluripotency in embryonic stem cells, and, *vice versa*, the substrates of pro-oxidative reactions (*e.g.,* acylcarnitines) promote neuronal and cardiac differentiation (48)

The PPP, a biochemical module within the central carbon metabolism, is of major importance in the chemical redox balance of the cell. When cells get in contact with an oxidant, this pathway is upregulated at the transcript, protein, enzyme-activity, and metabolite level (10, 16, 33, 37). As the oxidative part of the PPP reduces two $NADP^+$ molecules to NADPH for every metabolized glucose equivalent, this metabolic re-configuration provides the cellular antioxidative machinery (including glutathione and peroxiredoxin systems) with its primary redox cofactor (29, 49). This role of the PPP in the stress response is consistent with several experimental observations, including that the depletion of PPP enzymes can dramatically reduce the oxidant-resistance of yeast and other organisms (17).

The data presented here provide evidence for an additional, and NADP(H)-independent role of the PPP in the stress response. The LC-MS/MS measurements showed that intermediates of the nonoxidative PPP accumulate upon an oxidative treatment (33, 34), and the deletion of several nonoxidative PPP reactions impacts on the resistance against oxidants (17, 39).

We demonstrated that the deletion of a nonoxidative PPP enzyme (Tal1p) decreased oxidant sensitivity in a yeast strain that cannot use the PPP for $NADP^+$ reduction. *Vice versa*, increased flow into the nonoxidative PPP *via* the expression of a foreign enzyme (SHPK), which generates the PPP intermediate sedoheptulose-7P from the non-PPP metabolite sedoheptulose, increased yeast's H_2O_2 tolerance. Additionally, the exposure to different oxidants revealed divergent phenotypes among deletion strains of the oxidative and nonoxidative PPP branch. Testing three oxidants, we identified a phenotype for all assayed PPP enzyme knockouts. These phenotypes were specific, and occurred irrespectively whether the deleted enzyme was part of the oxidative and nonoxidative branch. All together, these results gave reason to postulate the existence of a second, NAPD(H)-independent function of the PPP in the stress response.

A unique feature of PPP activation is the speed at which this process occurs. An increase in the concentration of intermediate metabolites is detectable within seconds upon the cell's exposure to the oxidant (34). This rapid flux is triggered by the oxidative inactivation of at least one glycolytic enzyme, glyceraldehyde 3-phosphate dehydrogenase (GAPDH); GAPDH inactivation is completed within 10–15 s upon cellular contact with the oxidant (34) Both mathematical modeling and experimental results showed that GAPDH inactivation is capable to increase the concentration of PPP intermediates (33).

Transcriptional adaptation to oxidative conditions is much slower than this metabolic response. In yeast, early transcripts are induced ~2–3 min after exposure to the oxidant. All later transcriptional changes adhere to a strict timeline, resulting in characteristic time-courses for stress-induced mRNAs (7). A strong relation between the binding affinity of a transcription factor and the activation timing of its targets has been reported (6), but most mechanisms that are crucial for the dynamic timing of the stress program remain yet to be elucidated. A cell proceeds with its transcriptional program after the metabolic transition. Therefore, we considered that this process could be connected to the induction of transcriptional changes during the stress response. The comparison of mRNA expression profiles of yeast treated with oxidants and a TPI mutant with a constitutively activated PPP revealed that both conditions had a substantial overlap in their set of targets. Studying the expression of these genes in other PPP deletion strains demonstrated a PPP dependence of their transcriptional regulation.

Currently, the best understood sensing system detects a collapse in the redox state *via* oxidation of thiol groups in regulatory cysteines, present in oxidant-responsive transcription factors, or their binding proteins (3, 15, 41). The results presented here are consistent with this model, but also demonstrate that this current picture is still incomplete. The oxidation of sensory thiols cannot explain expression changes provoked by the activation of the PPP when no oxidant was added to the cells. For instance, one or more intermediates of the PPP could have a direct regulatory function and bind to stress responsive transcriptional regulators, thereby leading to their activation. The so-called reporter metabolites, metabolic intermediates with regulatory functions that entail transcriptional changes, have been found in several pathways, including glycolysis, but have not been discovered among PPP intermediates yet (12, 27). This assumption could be proven by the identification of one or more regulatory small molecule(s) among PPP intermediates, and by elucidating its/their interaction with the stress responsive regulome. An alternative possibility is classic, post-translational modifications and/or protein–protein interaction-based signaling cascades that might be initiated by a PPP enzyme. Such a mechanism, for instance, has been reported for GAPDH that activates mTOR signaling under conditions of high glycolytic flux. In the presence of high levels of the GAPDH substrate glyceraldehyde 3-phosphate, a complex between this enzyme and the mTOR activator Rheb is destabilized; released Rheb is then capable to activate the mTORC1 complex (23)

The primary targets of the metabolic transition were processes involved or directly dependent on energy metabolism. When PPP mutants were exposed to oxidants, transcripts related to ribosome biogenesis and translation [considered as the most energy-consuming processes of the cell (47)], subunits of the respiratory chain, and chromatin components did not show expression time-courses like in the wild-type strain.

This could have consequences on stress signaling, since dynamic changes in chromatin structure are central to mediating energy deprivation; histone modifications are under the direct control of the central carbon metabolism (46). Chromatin is central for spreading response to metabolic changes and stress (20). Heat stress, for instance, leads to a domain-wide displacement of histones. This stimulates the expression of heat shock genes independent from the activity of Swi/Snf transcriptional regulators (50). Similar processes are likely to play a role during the oxidative stress response and help the cell to establish and maintain a system-wide antioxidative response.

We provided examples of transcripts that were improperly regulated or timed upon the oxidant treatment of PPP-deficient yeast strains. For instance, *HHT1* mRNA levels are slightly decreased in the wild-type cells 3 min after exposure to the oxidant but reached the basal level 2 min later. The same process took much longer (15 min) in Δ*tal1* yeast (Fig. 4b). In most cases, the effects of the metabolic shift were strongest within the first 15 min after addition of the oxidant. This result matches the time-course of the metabolic transition itself, which has its amplitude quite early (~1 min) after an oxidative burst (34). The observations reveal that the metabolic transition plays its primary role in controlling gene regulation during early events of stress response. Later, this function may be taken over by other mechanisms. Indeed, some of the transition-responsive gene promoters contain binding sites for known oxidant-inactivated transcription factors [*e.g.,* the AP-1-like transcription factor *YAP1* (15)]. Thus, gene expression regulation by the metabolic shift (glycolysis/PPP) and redox-responsive transcription factors seem to be complementary and/or overlapping processes that are induced at a different kinetic. In this respect, it is possible that the PPP is involved in the regulation of gene expression upon a strong oxidative burst, but not during the endurance of chronic, low-level oxidative stress.

In summary, we demonstrated that a metabolic transition in central carbon metabolism is part of the cellular redox sensor and a regulatory component of the early antistress response. Not only does the increased metabolic activity of the PPP, a consequence of carbon flux rerouting that occurs upon the addition of a toxic oxidant concentration, increase the reduction rate of $NADP^+$, but at the same time, it is also required for accurate induction of the transcriptional stress response. Consequently, the PPP has a pivotal role upon an oxidative burst; it provides redox cofactors for the antioxidative machinery and is a regulator of gene expression (Fig. 5). This finding extends our knowledge regarding the induction of stress response with a dynamic, time-dependent system showing for the first time that a shift in a metabolic pathway is used to sense and transmit a stress stimulus. The current understanding of the dynamics in the cellular metabolome and the knowledge regarding functional interactions between small molecules of primary metabolism with regulatory macromolecules are still marginal. However, the dynamic nature of metabolic pathways make them ideal candidates to sense and control flexible systems, and, consequently, similar mechanisms could play a common

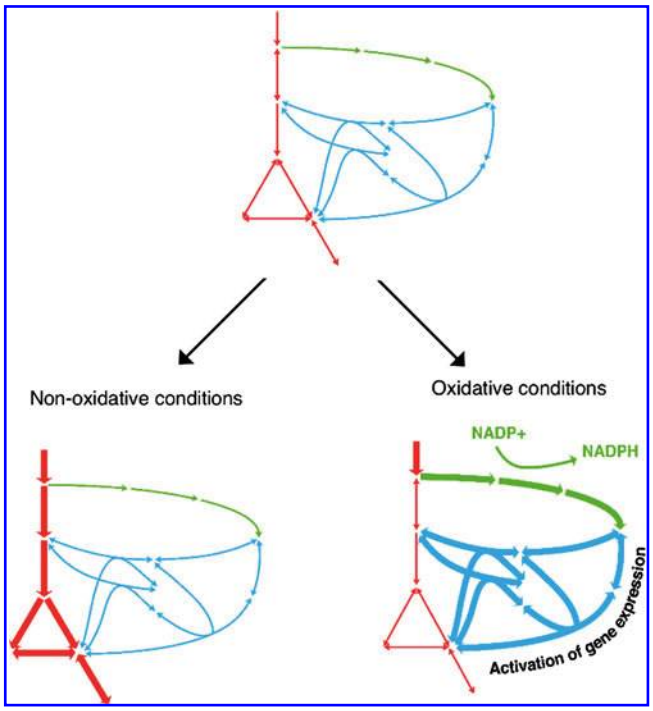

FIG. 5. The pivotal role of the PPP in the oxidative stress response. An oxidative burst activates the PPP. This yields NADPH as cofactor for the antioxidative machinery and glutathione recycling, and is simultaneously a metabolic signal that regulates gene expression during the stress response. (To see this illustration in color the reader is referred to the web version of this article at www.liebertonline.com/ars).

role in the regulation, fine-tuning, and timing of dynamic biological processes.

Materials and Methods

Yeast strain generation and cultivation

Yeast was cultivated in yeast-extract peptone dextrose (YPD; [20 g/l peptone BD Difco], 10 g/l yeast extract [BD Difco], 2% glucose) or synthetic complete (6.7 g/l yeast nitrogen base with ammonium sulfate [Wickerham formula; BD Difco], 0.59 g/l complete supplement mixture [CSM-ADE - HIS–LEU–TRP–URA, MPBiomedicals], 10 mg/ml adenine, 20 mg/l uracil, 20 mg/l histidine, 60 mg/l leucine, 40 mg/l tryptophan) agar (20 g/l), or liquid media at 28°C–30°C. Oxidant-bursts in liquid cultures were induced by adding H_2O_2 to a final concentration of 2 m*M*. BY4741 (S288c)-descendant yeast strains deleted for *ZWF1*, *TKL1*, *TAL1* (35), transgenic yeast expressing $TPI^{Ile170Val}$ (33), and low-level RPI (44) were described previously. *RPE1* and *TKL2* were deleted by a single-gene-replacement approach using the nourseothricin-resistance marker *natMX4*, and *SOL3/SOL4* using *kanMX4*. The *Δtal1Δzwf1* double mutant was generated by replacing *ZWF1* in the *Δtal1* yeast with *kanMX4*. Because a similar approach failed to create *Δtkl1Δzwf1* and *Δrpe1Δzwf1* double-knockouts, Tkl1p and Rpe1p were expressed from an *URA3* centromeric plasmid in *Δtkl1* or *Δrpe1* cells. *Δzwf1* was deleted in these transformants by single-gene replacement with *kanMX4*. Counter selection with 0.15% 5-fluoroorotic acid of *TKL1* or *RPE1* encoding *URA3* plasmids demonstrated a synthetic-lethal phenotype of *Δtkl1Δzwf1* and *Δrpe1Δzwf1* double-knockouts (Supplementary Fig. S1).

An *URA3* 2μ plasmid for the expression of GFP (p426GPD-GFP) was described earlier (32). The vector for the expression of SHPK was generated by PCR amplification of the mouse SHPK coding sequence from an *E. coli* expression plasmid (18) and sub-cloning it into the *URA3* 2μ vector p426GPD (25). The generated plasmid was verified by sequencing.

NADP(H) and NADPH measurements

For determination of the ratio of NADPH to the total NADP(H) concentration, yeast pellets were obtained from exponentially growing YPD cultures. Nucleotides were extracted by vigorous shaking of the frozen pellet on a FastPrep-24 machine (MP Biomedicals) after covering it with water:phenol:chloroform and zirconium beads. After centrifugation, the aqueous phase was transferred to a fresh tube and cleaned with phaselock gel (5Prime) to remove remaining organic solvent. Then, high-molecular components were removed by filtration through a 3-kDa-cutoff spinfilter (Millipore). NADPH and NADP(H) total concentrations in the filtrate were analyzed with a colorimetric $NADP^+$/NADPH assay kit (Abcam ab65349).

Expression profiling by deep sequencing of the transcriptome

For obtaining expression profiles, five yeast cultures (2 × BY4741, Δ*tal1*, Δ*tkl1*, and Δ*zwf1*) were grown in parallel in YPD media to mid-log phase. Thirty minutes before collecting the cells, H_2O_2 was added to one BY4741 culture to a final concentration of 2 m*M*. The cultures were centrifuged, pellets were washed, and total RNA was isolated using the RiboPure-Yeast kit (Ambion). mRNA was transcribed into cDNA and libraries for strand-specific Illumina sequencing were prepared as described earlier (26). In brief, $polyA^+$ RNA was purified with the Dynabeads mRNA purification kit

Table 2. Quantitative Real-Time–Polymerase Chain Reaction Primers

Gene product	*Forward primer*	*Reverse primer*
HHF1+2	GCCAAGCGTCACAGAAAGAT	GATGACGGATTCCAAGAAGG
HTA1+2	CCGGTGGTAAAGGTGGTAAA	AGACTGGAGCACCAGAACCA
HHT1+2	AAGGCTGCCAGAAAATCCGC	CTGACCAATCTTTGGAAAGG
HHO1	TAATGACGGTAAGGGCTCCA	GTTGCACTAACTCGCCGTTT
COX1+AI	TGCCTGCTTTAATTGGAGGT	CCCTGTACCAGCACCTGATT
COX2	GCTGATGTTATTCATGATTTTGC	TGGCATATTTGCATGACCTG
COX3	TCCATTCAGCTATGAGTCCTGA	ACCTGCGATTAAGGCATGAT
CIT1	TGGTTTAGCTGGCCCATTAC	ATGGCCATAACCAGGAACAA

Table 3. Multiple Reaction Monitoring Transitions

Protein	*Peptide*	*Quant. fragment*	*Q1 m/z*	*Q3 m/z*
Cit1p	ALSADLAAR	2y5	444.3	545.3
Cit1p	ALSADLAAR	2b8	444.3	713.4
Hht	YKPGTVALR	3y4	335.5	458.3
Hht	YKPGTVALR	3b5	335.5	547.3
Cox2p	NPIAYK	2y4	353.2	494.3
Cox2p	NPIAYK	2b5	353.2	559.3

(Invitrogen) following the manufacturer's instructions and treated with TURBO DNase (Ambion) (0.2 units per 1 μg of RNA) for 30 min at 37°C. The first-strand synthesis reaction was performed with 0.5 μg of polyA$^+$ RNA, d(N)6 primers and an oligo(dT) primer, reverse transcription buffer, dNTPs, $MgCl_2$, DTT, actinomycin D, RNase ,OUT'inhibitors, as well as SuperScript III reverse transcriptase (Invitrogen). dNTPs had been removed using a self-made 200 μl G-50 gel filtration spin-column (26) before the second strand was synthesized with DNA polymerase I as described.

Sequencing of the cDNA yielded 5–7-million paired-end reads (length 51 bp) and 10–14-million single reads. These reads were aligned using bowtie (22) on yeast genome SGD1.01 (www.ensembl.org/Saccharomyces_cerevisiae/Info/StatsTable?db=core). Only uniquely aligned reads we considered for calculating the expression profiles. To obtain gene expression levels (C), sequence reads falling within gene boundaries as defined in Ensemble 55 were counted. Then, their sum was normalized to a number of 10,000,000 for each profile, and the resulting quotient was used to normalize the individual transcript counts. To estimate the significance of divergence between a pair of genes, the pair-wise distances were calculated by the formula $D = \frac{C_1 - C_2}{\sqrt{\frac{1}{2}(C_1 + C_2)}}$, where C_1 and C_2 are the normalized counts on transcripts. A threshold of ± 5 was set for the comparison of *Δzwf1*, *Δtkl1*, and *Δtal1* profiles with transcripts of MR105 and H_2O_2 profiles; yeast transcripts falling within the top 5% boundary of pair-wise distance values were considered as significantly regulated.

Quantitative RT-PCR

Two μg total yeast RNA was transcribed into cDNA using a 12–18 oligo dT primer and Moloney Murine Leukemia virus (M-MuLV) reverse transcriptase (NEB) according to the manufacturer's instructions. qRT-PCR were performed on an Prism 7900HT cycler (Applied Biosystems) with gene-specific primers (Table 2) as described previously (44). The relative expression ratio of the target genes was normalized to the geometric mean of the three endogenous references genes (*ACN9*, *ATG27*, and *TAF10*) by the method of Pfaffl (28). Each assay was performed in independent triplicate runs with templates from independent reverse transcription reactions.

Quantitative mass spectrometry

Sugar-phosphate intermediates were quantified by LC-MS/MS as described by Wamelink *et al.* (43). In brief, metabolites were extracted in Hanks balanced salt solution containing 2% perchloric acid, and spiked with an isotope-labeled internal standard ($^{13}C_6$-glucose-6P). Proteins were precipitated after neutralization with a phosphate buffer. Then, samples were then separated with a linear water/acetonitrile gradient using octylammonium acetate (500 mg/l, pH 7.5) ion pairing reagent on a C_{18} column at a flow rate of 1 ml/min. The on-line coupling of the HPLC system to an API-3000 mass spectrometer (AB/Sciex), operating in MRM mode, allowed quantification of sugar-phosphate intermediates.

Peptide quantification was conducted on a hybrid triple quadrupole/ion trap mass spectrometer coupled to a 2D ultra nanoLC (Eksigent) as described previously (2). In brief, whole yeast protein extracts were digested with trypsin and separated with a 90 min water/acetonitrile gradient on a Zorbax 300SB-C_{18}, 0.0075 × 150 mm column (Agilent) at a flow rate of 300nl/min. Quantification was carried out on a QTRAP5500 (AB/Sciex) instrument equipped with Nanospray III ion source (AB/Sciex) operating in MRM mode. Each peptide was quantified with two MRM transitions and internally normalized to a tryptic peptide of 60S ribosomal protein L36-B (RPL36B). MRM (Q1/Q3) transitions are given in Table 3.

Acknowledgments

The authors would like to thank Beata Lukaszewska-McGreal, Erwin Jansen, and Serkan Ceyhan for help with mass spectrometry and sample preparation, our lab members for critical discussions, and Emile van Schaftingen (Université catholique de Louvain) for providing a mouse SHPK plasmid. Part of this work was funded by the Max Planck society.

Author Disclosure Statement

All authors declare that no competing financial interests exist.

References

1. Arya R, Lalloz MR, Bellingham AJ, and Layton DM. Evidence for founder effect of the Glu104Asp substitution and identification of new mutations in triosephosphate isomerase deficiency. *Hum Mutat* 10: 290–294, 1997.
2. Bluemlein K and Ralser M. Monitoring protein expression in whole-cell extracts by targeted label- and standard-free LC-MS/MS. *Nat Protoc* 6: 2011.
3. Brandes N, Schmitt S, and Jakob U. Thiol-based redox switches in eukaryotic proteins. *Antioxid Redox Signal* 11: 997–1014, 2008.
4. Castegna A, Scarcia P, Agrimi G, Palmieri L, Rottensteiner H, Spera I, Germinario L, and Palmieri F. Identification and functional characterization of a novel mitochondrial carrier for citrate and oxoglutarate in Saccharomyces cerevisiae. *J Biol Chem* 285: 17359–17370, 2010.

5. Castrillo JI, Zeef LA, Hoyle DC, Zhang N, Hayes A, Gardner DC, Cornell MJ, Petty J, Hakes L, Wardleworth L, Rash B, Brown M, Dunn WB, Broadhurst D, O'Donoghue K, Hester SS, Dunkley TP, Hart SR, Swainston N, Li P, Gaskell SJ, Paton NW, Lilley KS, Kell DB, and Oliver SG. Growth control of the eukaryote cell: a systems biology study in yeast. *J Biol* 6: 4, 2007.
6. Chechik G and Koller D. Timing of gene expression responses to environmental changes. *J Comput Biol* 16: 279–290, 2009.
7. Chechik G, Oh E, Rando O, Weissman J, Regev A, and Koller D. Activity motifs reveal principles of timing in transcriptional control of the yeast metabolic network. *Nat Biotechnol* 26: 1251–1259, 2008.
8. Demple B and Amabile-Cuevas CF. Redox redux: the control of oxidative stress responses. *Cell* 67: 837–839, 1991.
9. Finkel T and Holbrook NJ. Oxidants, oxidative stress and the biology of ageing. *Nature* 408: 239–247, 2000.
10. Godon C, Lagniel G, Lee J, Buhler JM, Kieffer S, Perrot M, Boucherie H, Toledano MB, and Labarre J. The H2O2 stimulon in Saccharomyces cerevisiae. *J Biol Chem* 273: 22480–22489, 1998.
11. Grant CM. Metabolic reconfiguration is a regulated response to oxidative stress. *J Biol* 7: 1, 2008.
12. Gruning NM, Lehrach H, and Ralser M. Regulatory crosstalk of the metabolic network. *Trends Biochem Sci* 35: 220–227, 2010.
13. Heinemann M and Sauer U. Systems biology of microbial metabolism. *Curr Opin Microbiol* 13: 337–343, 2010.
14. Ho HY, Cheng ML, Lu FJ, Chou YH, Stern A, Liang CM, and Chiu DT. Enhanced oxidative stress and accelerated cellular senescence in glucose-6-phosphate dehydrogenase (G6PD)-deficient human fibroblasts. *Free Radic Biol Med* 29: 156–169, 2000.
15. Ikner A and Shiozaki K. Yeast signaling pathways in the oxidative stress response. *Mutat Res* 569: 13–27, 2005.
16. Janero DR, Hreniuk D, and Sharif HM. Hydroperoxide-induced oxidative stress impairs heart muscle cell carbohydrate metabolism. *Am J Physiol* 266: C179–C188, 1994.
17. Juhnke H, Krems B, Kotter P, and Entian KD. Mutants that show increased sensitivity to hydrogen peroxide reveal an important role for the pentose phosphate pathway in protection of yeast against oxidative stress. *Mol Gen Genet* 252: 456–464, 1996.
18. Kardon T, Stroobant V, Veiga-da-Cunha M, and Schaftingen EV. Characterization of mammalian sedoheptulokinase and mechanism of formation of erythritol in sedoheptulokinase deficiency. *FEBS Lett* 582: 3330–3334, 2008.
19. Kennell JC, Moran JV, Perlman PS, Butow RA, and Lambowitz AM. Reverse transcriptase activity associated with maturase-encoding group II introns in yeast mitochondria. *Cell* 73: 133–146, 1993.
20. Ladurner AG. Rheostat control of gene expression by metabolites. *Mol Cell* 24: 1–11, 2006.
21. Landriscina M, Maddalena F, Laudiero G, and Esposito F. Adaptation to oxidative stress, chemoresistance, and cell survival. *Antioxid Redox Signal* 11: 2701–2716, 2009.
22. Langmead B, Trapnell C, Pop M, and Salzberg SL. Ultrafast and memory-efficient alignment of short DNA sequences to the human genome. *Genome Biol* 10: R25, 2009.
23. Lee MN, Ha SH, Kim J, Koh A, Lee CS, Kim JH, Jeon H, Kim DH, Suh PG, and Ryu SH. Glycolytic flux signals to mTOR through glyceraldehyde-3-phosphate dehydrogenase-mediated regulation of Rheb. *Mol Cell Biol* 29: 3991–4001, 2009.
24. Mary J, Vougier S, Picot CR, Perichon M, Petropoulos I, and Friguet B. Enzymatic reactions involved in the repair of oxidized proteins. *Exp Gerontol* 39: 1117–1123, 2004.
25. Mumberg D, Muller R, and Funk M. Yeast vectors for the controlled expression of heterologous proteins in different genetic backgrounds. *Gene* 156: 119–122, 1995.
26. Parkhomchuk D, Borodina T, Amstislavskiy V, Banaru M, Hallen L, Krobitsch S, Lehrach H, and Soldatov A. Transcriptome analysis by strand-specific sequencing of complementary DNA. *Nucleic Acids Res* 37: e23, 2009.
27. Patil KR and Nielsen J. Uncovering transcriptional regulation of metabolism by using metabolic network topology. *Proc Natl Acad Sci U S A* 102: 2685–2689, 2005.
28. Pfaffl MW. A new mathematical model for relative quantification in real-time RT-PCR. *Nucleic Acids Res* 29: e45, 2001.
29. Pollak N, Dolle C, and Ziegler M. The power to reduce: pyridine nucleotides—small molecules with a multitude of functions. *Biochem J* 402: 205–218, 2007.
30. Rajasekaran NS, Connell P, Christians ES, Yan LJ, Taylor RP, Orosz A, Zhang XQ, Stevenson TJ, Peshock RM, Leopold JA, Barry WH, Loscalzo J, Odelberg SJ, and Benjamin IJ. Human alpha B-crystallin mutation causes oxido-reductive stress and protein aggregation cardiomyopathy in mice. *Cell* 130: 427–439, 2007.
31. Ralser M, Heeren G, Breitenbach M, Lehrach H, and Krobitsch S. Triose phosphate isomerase deficiency is caused by altered dimerization-not catalytic inactivity-of the mutant enzymes. *PLoS ONE* 1: e30, 2006.
32. Ralser M, Nonhoff U, Albrecht M, Lengauer T, Wanker EE, Lehrach H, and Krobitsch S. Ataxin-2 and huntingtin interact with endophilin-A complexes to function in plastin-associated pathways. *Hum Mol Genet* 14: 2893–2909, 2005.
33. Ralser M, Wamelink MM, Kowald A, Gerisch B, Heeren G, Struys EA, Klipp E, Jakobs C, Breitenbach M, Lehrach H, and Krobitsch S. Dynamic rerouting of the carbohydrate flux is key to counteracting oxidative stress. *J Biol* 6: 10, 2007.
34. Ralser M, Wamelink MM, Latkolik S, Jansen EE, Lehrach H, and Jakobs C. Metabolic reconfiguration precedes transcriptional regulation in the antioxidant response. *Nat Biotechnol* 27: 604–605, 2009.
35. Ralser M, Wamelink MM, Struys EA, Joppich C, Krobitsch S, Jakobs C, and Lehrach H. A catabolic block does not sufficiently explain how 2-deoxy-D-glucose inhibits cell growth. *Proc Natl Acad Sci U S A* 105: 17807–17811, 2008.
36. Schulz TJ, Zarse K, Voigt A, Urban N, Birringer M, and Ristow M. Glucose restriction extends *Caenorhabditis elegans* life span by inducing mitochondrial respiration and increasing oxidative stress. *Cell Metab* 6: 280–293, 2007.
37. Shenton D and Grant CM. Protein S-thiolation targets glycolysis and protein synthesis in response to oxidative stress in the yeast Saccharomyces cerevisiae. *Biochem J* 374: 513–519, 2003.
38. Sies H. Oxidative stress: oxidants and antioxidants. *Exp Physiol* 82: 291–295, 1997.
39. Thorpe GW, Fong CS, Alic N, Higgins VJ, and Dawes IW. Cells have distinct mechanisms to maintain protection against different reactive oxygen species: oxidative-stress-response genes. *Proc Natl Acad Sci U S A* 101: 6564–6569, 2004.
40. Ugarte N, Petropoulos I, and Friguet B. Oxidized mitochondrial protein degradation and repair in aging and oxidative stress. *Antioxid Redox Signal* 13: 539–549, 2010.
41. Veal EA, Day AM, and Morgan BA. Hydrogen peroxide sensing and signaling. *Mol Cell* 26: 1–14, 2007.
42. Verho R, Richard P, Jonson PH, Sundqvist L, Londesborough J, and Penttila M. Identification of the first fungal NADP-GAPDH from Kluyveromyces lactis. *Biochemistry* 41: 13833–13838, 2002.

43. Wamelink M, Jansen E, Struys E, Lehrach H, Jakobs C, and Ralser M. Quantification of *Saccharomyces cerevisiae* pentose-phosphate pathway intermediates by LC-MS/MS. *Nat Protoc Netw* 10.1038/nprot.2009.140, 2009.
44. Wamelink MM, Grüning NM, Jansen EE, Bluemlein K, Lehrach H, Jakobs C, and Ralser M. The difference between rare and exceptionally rare: molecular characterization of ribose 5-phosphate isomerase deficiency. *J Mol Med* 88: 931–939, 2010.
45. Wamelink MM, Struys EA, and Jakobs C. The biochemistry, metabolism and inherited defects of the pentose phosphate pathway: a review. *J Inherit Metab Dis* 31: 703–717, 2008.
46. Wellen KE, Hatzivassiliou G, Sachdeva UM, Bui TV, Cross JR, and Thompson CB. ATP-citrate lyase links cellular metabolism to histone acetylation. *Science* 324: 1076–1080, 2009.
47. Wilson DN and Nierhaus KH. The weird and wonderful world of bacterial ribosome regulation. *Crit Rev Biochem Mol Biol* 42: 187–219, 2007.
48. Yanes O, Clark J, Wong DM, Patti GJ, Sanchez-Ruiz A, Benton HP, Trauger SA, Desponts C, Ding S, and Siuzdak G. Metabolic oxidation regulates embryonic stem cell differentiation. *Nat Chem Biol* 6: 411–417, 2010.
49. Ying W. NAD+/NADH and NADP+/NADPH in cellular functions and cell death: regulation and biological consequences. *Antioxid Redox Signal* 10: 179–206, 2008.
50. Zhao J, Herrera-Diaz J, and Gross DS. Domain-wide displacement of histones by activated heat shock factor occurs independently of Swi/Snf and is not correlated with RNA polymerase II density. *Mol Cell Biol* 25: 8985–8999, 2005.

Address correspondence to:
Dr. Markus Ralser
Department of Biochemistry
Cambridge Systems Biology Centre
University of Cambridge
Sanger Building
50 Tennis Court Road
Cambridge CB2 1GA
United Kingdom

E-mail: ralser@molgen.mpg.de

Date of first submission to ARS Central, November 26, 2010; date of final revised submission, February 16, 2011; date of acceptance, February 19, 2011.

Abbreviations Used

CHP = cumene-hydroperoxide
DTT = dithiothreitol
GO = gene ontology
Gpx = glutathione peroxidase
H_2O_2 = hydrogen peroxide
LC-MS/MS = liquid chromatography tandem mass spectrometry
MRM = multiple reaction monitoring
PPP = pentose phosphate pathway
RPI = ribulose 5-phosphate isomerase
SHPK = sedoheptulokinase
YPD = yeast-extract peptone dextrose

This article has been cited by:

1. Weibo Luo, Gregg L. Semenza. 2012. Emerging roles of PKM2 in cell metabolism and cancer progression. *Trends in Endocrinology & Metabolism* **23**:11, 560-566. [CrossRef]
2. Zuzana Hodurova, Laura Ferreira, Fernando Sánchez-Juanes, Angel Dominguez, Yvetta Gbelska. 2012. Cytosolic proteome of Kluyveromyces lactis affected by the multidrug resistance regulating transcription factor KlPdr1p. *Journal of Proteomics* **75**:17, 5316-5326. [CrossRef]
3. Julia Ring, Cornelia Sommer, Didac Carmona-Gutierrez, Christoph Ruckenstuhl, Tobias Eisenberg, Frank Madeo. 2012. The metabolism beyond programmed cell death in yeast. *Experimental Cell Research* **318**:11, 1193-1200. [CrossRef]
4. Nana-Maria Grüning, Markus Ralser. 2011. Cancer: Sacrifice for survival. *Nature* **480**:7376, 190-191. [CrossRef]
5. Nana-Maria Grüning, Mark Rinnerthaler, Katharina Bluemlein, Michael Mülleder, Mirjam M.C. Wamelink, Hans Lehrach, Cornelis Jakobs, Michael Breitenbach, Markus Ralser. 2011. Pyruvate Kinase Triggers a Metabolic Feedback Loop that Controls Redox Metabolism in Respiring Cells. *Cell Metabolism* **14**:3, 415-427. [CrossRef]